Understanding ferrite deformation caused by austenite to martensite transformation in dual phase steels

Atreya, V.; Bos, C.; Santofimia, Maria Jesus

DOI
10.1016/j.scriptamat.2021.114032

Publication date
2021

Document Version
Final published version

Published in
Scripta Materialia

Scripta Materialia 202 (2021) 114032

Contents lists available at ScienceDirect

Scripta Materialia

journal homepage: www.elsevier.com/locate/scriptamat

Understanding ferrite deformation caused by austenite to martensite transformation in dual phase steels

Vibhor Atreya[a,*], Cornelis Bos[a,b], Maria J. Santofimia[a]

[a] Department of Materials Science and Engineering, Delft University of Technology, 2628CD Delft, The Netherlands
[b] Tata Steel R&D, IJmuiden, The Netherlands

ARTICLE INFO

Article history:
Received 4 March 2021
Revised 19 May 2021
Accepted 25 May 2021

Keywords:
Electron backscattering diffraction (EBSD)
dual phases steels
martensitic phase transformation
plastic deformation
slip transmission

ABSTRACT

During the production of DP steels, the volume expansion and shape change accompanying the austenite to martensite transformation is accommodated by the deformation of surrounding ferrite grains. The extent of the deformation in ferrite grains ultimately affects the mechanical properties of DP steels. Using electron backscatter diffraction measurements, this study identifies the characteristics of martensite which govern the extent of transformation induced deformation of ferrite grains. It was found that small austenite grains tend to transform into martensitic variants having a close-packed plane parallel relationship with adjacent ferrite grains, thus achieving relatively easy slip transmission and resulting in a long-range deformation of ferrite grains. Ferrite grains can also exhibit a short-range deformation limited to the vicinity of the ferrite/martensite interface, which is primarily governed by martensite carbon content.

Dual-Phase (DP) steels belong to the first generation of advanced high strength steels (AHSS) [1] and are widely used in the automotive industry. DP steels consist of hard martensite particles dispersed in a soft ferritic matrix, leading to a good combination of strength and ductility [1–3]. In DP steels, martensite is typically formed from the austenite present in an intercritical ferrite-austenite microstructure during rapid cooling to room temperature. Martensite formation includes volume expansion and shape change, which takes place through dilatation and shearing of the prior austenite region.

To accommodate the volume expansion and shape change of newly formed martensite, the surrounding ferrite grains undergo deformation. Stresses generated as a result of this deformation can locally exceed the elastic limit of ferrite, thus causing plastic deformation [4–7]. High elastic stresses can persist in the ferrite matrix even after the transformation-induced plastic deformation has ceased.

These plastically deformed ferrite regions contain mobile dislocations as reported by previous studies [1,6–9]. These dislocations, aided by high internal elastic stresses, can move under low macroscopic stress and interact to produce a high initial work hardening rate. Thus, yielding in DP steels starts quite early in the form of localized plasticity. This leads to the absence of a sharp yield point in a typical uniaxial tensile stress-strain curve, a phenomenon known as continuous yielding [10–12]. The mechanical behavior of DP steels thus depends upon the extent of transformation induced deformation of ferrite.

Earlier investigations attempted to relate the extent of a ferrite grain deformation to local microstructural aspects such as the fraction of ferrite/martensite phase boundary in the ferrite grain [13], its adjoining martensite island size, and the strength of the ferrite grain itself [14–17]. However, the extent to which different ferrite grains in the specimen deform could not be fully explained based on the aforementioned microstructural aspects only [18]. Several characteristics of martensite in DP steels need to be examined in order to fully understand how martensite formation causes the surrounding ferrite grains to deform.

In this work, transformation induced deformation of ferrite is investigated considering martensite volume fraction, the carbon content of martensite, martensite sub-structure size, and relative orientation between deformed ferrite grains and its adjacent martensite.

The starting material consisted of cold rolled steel with a ferrite-pearlite microstructure and composition 0.14C-1.8Mn-0.24Si by weight%. Three specimens with dimensions 10 mm x 4 mm x 2 mm were cut from the material using electrical discharge machining (EDM) and heat-treated in a Bahr DIL 805 A/D dilatometer. Specimens were heated with a rate of 5 K/s and kept at intercrit-

* Corresponding author.
E-mail address: V.Atreya@tudelft.nl (V. Atreya).

https://doi.org/10.1016/j.scriptamat.2021.114032

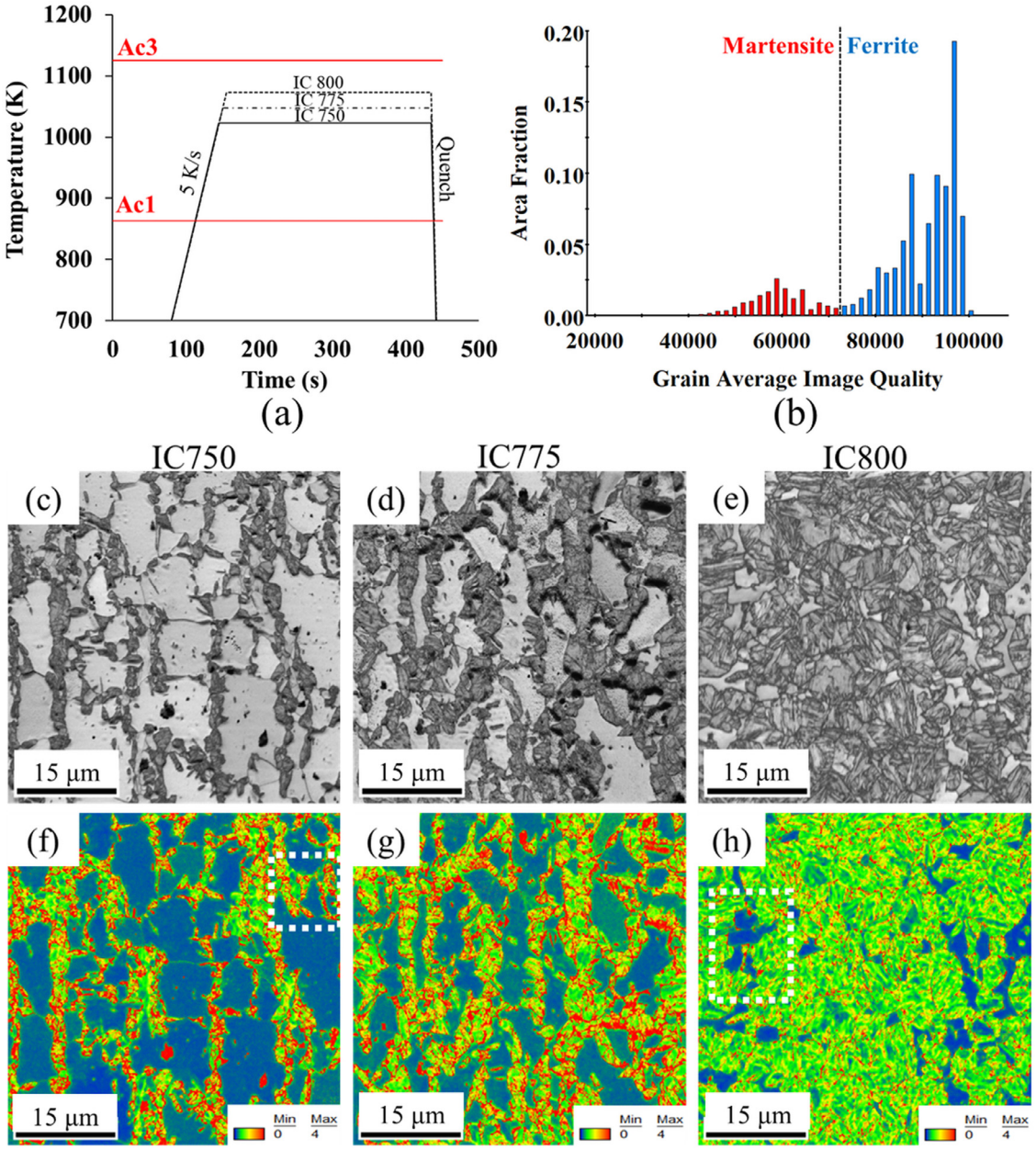

Fig. 1. (a) Applied heat treatments on specimens. Ac1 and Ac3 refer to critical temperatures indicating beginning and end of austenite formation, determined from dilatometry curve of a steel specimen heated to full austenitization; (b) Grain average image quality (GAIQ) distribution showing martensite and ferrite peaks; (c, d, e) EBSD image quality (IQ) maps for specimens IC750, IC775, and IC800; (f, g, h) EBSD kernel average misorientation (KAM) maps for specimens IC750, IC775, and IC800.

ical temperature for 5 min to obtain different phase fractions of austenite and ferrite, followed by quenching to fully transform the austenite to martensite. The heat treatment regimes are shown in Fig. 1(a). The specimens are named IC750, IC775, and IC800 where the last three digits denote the intercritical annealing temperatures in Celsius. All specimens were then ground using SiC abrasive papers and polished with 3 and 1-micron diamond paste followed by electro-polishing using Struers electrolyte A2 at 35V, 277 K for 6s to prepare them for electron backscatter diffraction (EBSD) measurements. EBSD maps were taken on a Zeiss Ultra 55 machine equipped with a Field Emission Gun Scanning Electron Microscope (FEG-SEM) using Edax Pegasus XM 4 Hikari EBSD system. The scan area for this study was 50 μm x 50 μm, with a step size of 50 nm.

The TSL OIM version 7 software was used to analyze the EBSD scans. To quantify phase fractions, the grain average image quality (GAIQ) measure was used. GAIQ is the average of image quality values of all points belonging to a grain. Using a grain tolerance angle value between 0.5°-1.5° to demarcate grains for GAIQ calculation enables excellent identification of martensite particles in ferrite-martensite DP microstructures [19,20]. The difference between GAIQ peaks obtained for ferrite and martensite is illustrated in Fig. 1(b). Martensite phase fractions calculated by this method for analyzed EBSD locations are 0.33, 0.56, 0.93 for IC750, IC775, and IC800 respectively.

Fig. 1 (c, d, e) shows the image quality (IQ) maps of all specimens obtained via EBSD. Ferrite regions have better image quality and appear light grey in EBSD image quality (IQ) maps as compared to martensite regions which appear dark grey [1,20]. The martensite particles resemble connected chains in IC750 and IC775, with the chains being bulkier in IC775.

Fig. 1 (f, g, h) shows the kernel average misorientation (KAM) maps of all specimens. The KAM measure gives an estimate of the

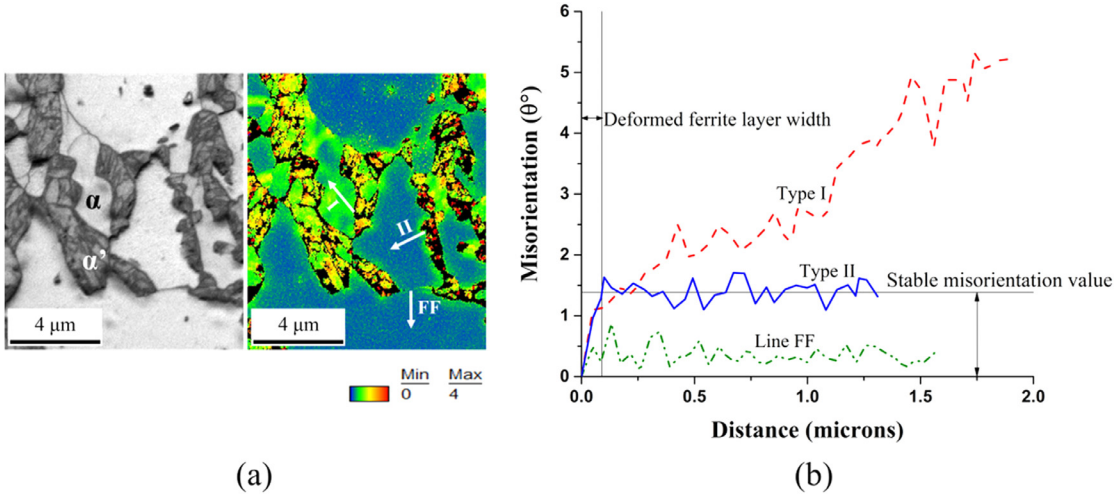

Fig. 2. (a) IQ and KAM maps of ferrite grains F1 and F2 from the region of IC750 specimen highlighted in figure 1(f) with three profile lines. FF starts from the ferrite/ferrite phase boundary whereas lines I and II start from the ferrite/martensite phase boundary. Black regions in the KAM map represent pixels with low confidence index (b) Change in point-to-origin misorientation angle while moving along profile line from phase/grain boundary towards ferrite grain interior.

extent of deformation within a grain [21,22,23,24]. The n^{th} kernel average misorientation (KAM) at a point is defined as the average misorientation of that point with respect to the 'n' numbers of nearest neighbors, neglecting the ones above a certain threshold misorientation. In the figure, KAM maps are shown for the 5^{th} nearest neighbor and a maximum 4° misorientation. The blue and the red end of the colored spectrum denote the minimum and maximum KAM values respectively. Martensite regions appear red in KAM maps due to very high misorientations, while the ferrite regions appear blue. There is a higher number of ferrite grains with deformation in IC750 and IC775 than in IC800. No prominent deformation is seen in the ferrite grains of IC800.

It is observed that some ferrite grains undergo long-range deformation, while in others deformation is limited to the vicinity of phase boundaries. This is evident from misorientation gradients present within the ferrite grains. For a detailed study, EBSD data subsets from the regions of interest were cleaned using the neighbor confidence index (CI) correlation tool, and points with CI less than 0.1 were removed. Further cleaning was avoided. Fig. 2(a) shows the IQ and KAM maps of ferrite grains labeled F1 and F2 from the region of the IC750 specimen highlighted in Fig. 1(f). In the ferrite grain F1, KAM gradients cover the majority of the grain area. In the ferrite grain F2, higher KAM values are confined to the vicinity of the ferrite/martensite phase boundary in the form of a layer of deformed ferrite.

For a clear illustration, three misorientation profile lines are drawn in Fig. 2(a). Changes in misorientation angle with respect to the origin along the profile lines are plotted in Fig. 2(b). For the profile line which starts from ferrite/ferrite grain boundary (FF), the misorientation angle in Fig. 2(b) first increases up to a certain distance and then becomes nearly stable. For the profile lines which start at the ferrite/martensite (FM) phase boundary, there are two scenarios: type I and II. In the type I profile line, the corresponding misorientation angle in Fig. 2(b) shows a continuously increasing trend even at a distance equal to half the grain size. This indicates that the grain has undergone significant deformation in its interior. Such deformation is henceforth called type I long range (type I LR in short) ferrite deformation.

In the type II profile line, the misorientation angle change behaves similarly to that of the first case (FF), except that the stable misorientation value is significantly higher. This indicates that the deformation in ferrite grain is highest near the phase boundary and decreases up to a certain distance which represents the deformed ferrite layer width. The deformation remains confined to a small region near the phase boundary. This type of deformation is henceforth called type II short range (type II SR in short) ferrite deformation.

The occurrence of ferrite grains with type I LR deformation is common in EBSD scans of IC750 and rare in IC775. Type II SR deformation can be spotted in several grains in both IC750 and IC775. However, in IC800, both type I LR and type II SR deformation appear to be absent.

Grains with type I LR deformation were quantified using the grain orientation spread (GOS) measure. It is used to estimate deformation in grains, especially to distinguish non-recrystallized grains from recrystallized ones [25]. For calculating GOS, the average orientation of the grain is calculated. Then the misorientations between this average orientation and the orientation of each measurement point within the grain are calculated. The average of these misorientations is the GOS value of that grain. Grains with type II SR deformation were quantified by identifying grains with a discernable width of deformed ferrite layer as illustrated in Fig. 2(b).

Volume fractions of ferrite grains with different types of deformation quantified from EBSD scans of Fig. 1(c-h) are shown in Fig. 3(a) together with the volume fraction of martensite. The deformed ferrite layer width for type II SR deformation measured for several randomly selected ferrite grains of IC750 and IC775 was found to be in the range 0.1 μm - 0.5 μm, while in IC800 it is absent, as evident from Fig. 3(b).

It is important to note that type II SR deformation in a ferrite grain can occur in addition to type I LR deformation. The large KAM gradients from type I LR deformation obfuscate the gradients showing the deformed ferrite layer formed due to type II SR deformation. Therefore, it is highly likely that some fraction of ferrite grains exhibiting type I LR deformation contain type II SR deformation too.

To investigate its influence on transformation induced ferrite deformation, the carbon content of martensite was calculated using the carbon mass balance equation, $C_0 = V_f C_f + V_m C_m$, where $C_0 = 0.13$ wt.% is the mean steel carbon content, V_f, V_m are the volume fractions of ferrite and martensite, C_f, C_m are the carbon contents of ferrite and martensite in wt.% respectively. The values of C_f were approximated as the equilibrium carbon content in ferrite at different intercritical temperatures. This was calculated in ThermoCalc software using the TCFe9 database.

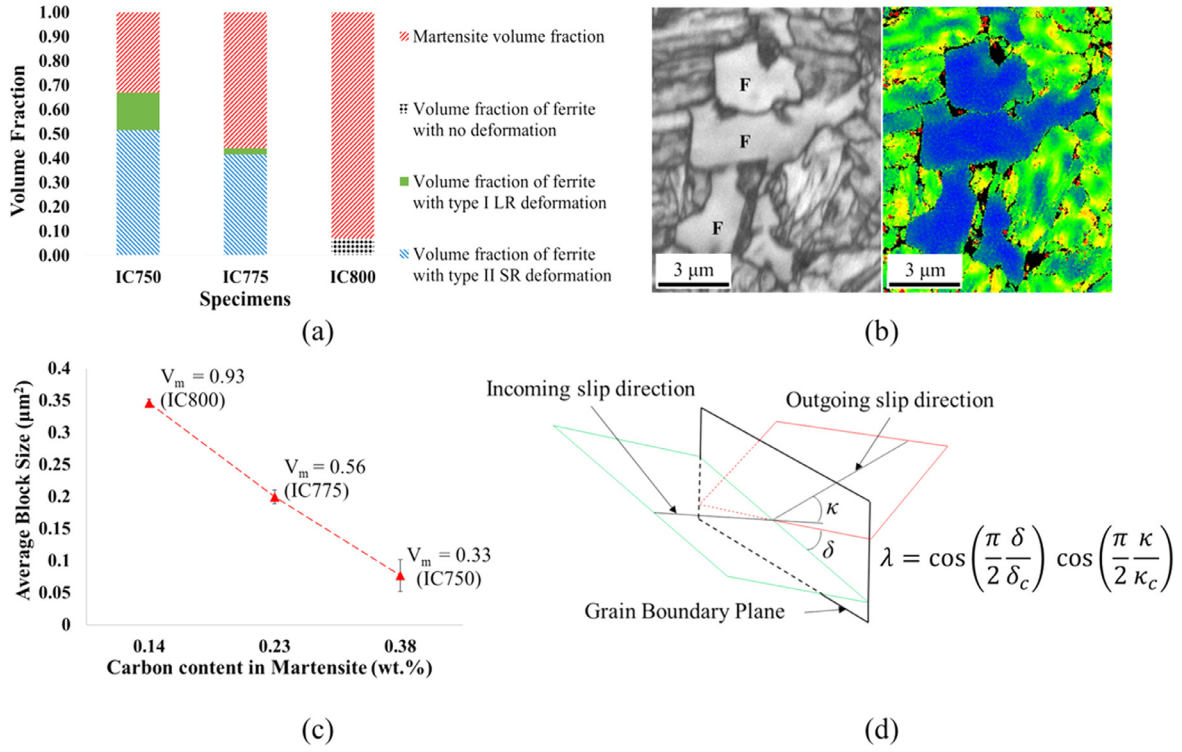

Fig. 3. (a) Volume fraction of martensite and different types of ferrite deformation based on EBSD scans of figure 1(c-h); (b) IQ and KAM map of a region of IC800 highlighted in figure 1(h) with some ferrite grains indicated with 'F'. Both type I and type II deformation are absent (c) Variation in average block size and carbon content of martensite for specimens with different martensite volume fraction (V_m) *(d)* Geometrical configuration of slip planes during slip transmission. Incoming and outgoing slip planes are indicated in green and red colors respectively. The equation for slip transfer number λ is shown, where δ is the angle between the lines of intersection of slip planes with the boundary plane, κ is the angle between slip directions, δ_c and κ_c are the limiting values of δ and κ beyond which slip transmission is unlikely.

Fig. 3(c) shows the variation of average block size with carbon content in martensite for different martensite volume fractions. It shows that an increase in carbon content reduces the martensite sub-structure size, as reported in the literature [26,27]. It can also be inferred that IC750 must have had the smallest average prior austenite grain size (PAGS) among all specimens since the average block size of martensite is directly proportional to the average PAGS of the specimen [28–30].

A potential explanation for the transformation-induced type I LR deformation of ferrite is slip transmission. Slip transmission from martensite to adjacent austenite [31] or ferrite grains [32] has been reported in the literature. Grain boundaries block dislocation movement, hence providing material strengthening [33,34]. However, there can be partial or even full transmission of dislocations across the grain or phase boundaries under certain conditions.

The geometrical criteria used to estimate ease of slip transmission is called the slip transfer number λ [35,36] which is a function of δ - the angle between the lines of intersection of slip planes with the boundary plane, and κ - the angle between slip directions, or burgers vectors as shown in Fig. 3(d). The smaller the values of δ and κ, the higher the value of λ and greater is the slip transmission. If the planes and directions of incoming and outgoing slip are nearly parallel, there is a greater chance of slip transmission [37].

Since the (110) plane is the most active slip plane for bcc crystal structures, the (110) pole figures were plotted for ferrite grains F1 and F2 of Fig. 2(a) and overlaid on (110) pole figures of adjacent martensite blocks to check for parallel plane relationships [32,38], as shown in Fig. 4(a) and (b). Overlap in pole figures (highlighted by black circles) shows that the (110) planes of the ferrite grains with type I LR deformation exhibit a parallel relationship with the (110) planes of adjacent martensite blocks. Such a relationship is henceforth referred to as (110) close packed plane parallel (CPPP) relationship. The martensite blocks which show (110) CPPP relationship with the ferrite grain are colored.

The requirement of angle κ for ease of slip transmission is less strict than δ [35]. 5 out of a total of 10 martensite blocks with a CPPP relationship have at least one <111> direction parallel to the <111> direction of ferrite grain F1, indicated by the black circle in (111) pole figures shown in Fig. 4(a). The rest of the blocks have a misorientation of 5°-15° between their <111> direction and <111> direction of ferrite, which is lower than the generally used critical value of κ ($\kappa_c = 45°$), above which slip transmission is not possible [35]. Such blocks are indicated by a dotted black circle in (111) pole figure shown in Fig. 4(a).

Ferrite grain F2 which shows type II SR deformation only has one small martensite block with (110) CPPP relationship. On the contrary, a higher number of martensite blocks with (110) CPPP relationship are present adjacent to type I LR deformed ferrite grain F1. The quantification of grains that show CPPP relation for all three specimen scans is given in table 1. The volume fraction of ferrite grains with type I LR deformation and also exhibiting CPPP relation is highest in IC750.

In 2D micrographs, it is always a concern whether observations may have been influenced by features below the surface. The amount of ferrite exhibiting type I LR deformation as a percentage of total ferrite is 24%, 7%, and 0% for IC750, IC775, and IC800 respectively. This indicates that observations of type I LR deformation cannot be caused solely by the presence of martensite beneath the ferrite grain observed in the 2D scan as in that case an equal fraction of ferrite grains should have exhibited type I LR deformation in all specimens.

The highest frequency of type I LR deformed ferrite grains in IC750 can be explained as follows. IC750 has the minimum average

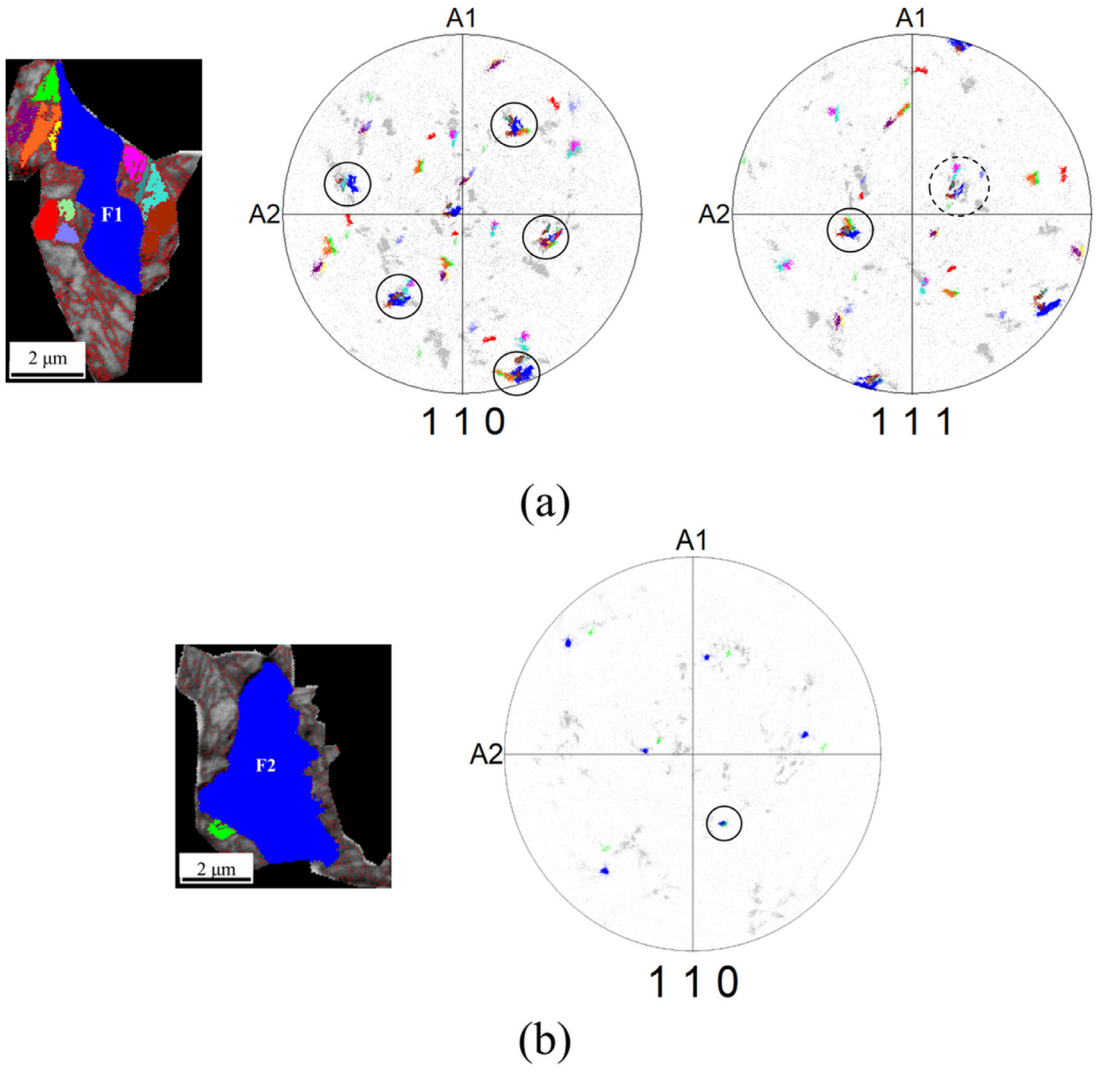

Fig. 4. IQ maps and (110) pole figures of ferrite grains (a)F1 and (b) F2 (both highlighted in blue in IQ maps above) in specimen IC750 exhibiting type I and type II deformations respectively, overlaid on (110) pole figures of surrounding martensite blocks (grey colored points). The blocks showing the CPPP relationship with ferrite are colored in IQ maps along with corresponding points on the pole figure. Black circles indicate overlapping 110 planes of ferrite and martensite blocks. In (a), (111) pole figures show the <111> directions in ferrite grain F1 overlaid on those of highlighted martensite blocks. Black circle indicates overlapping <111> directions for effective slip transfer. Dotted black circle indicate those blocks which have 5°-15° misorientation between their <111> direction and <111> direction of ferrite.

Table 1
Quantification of type I LR ferrite grains with CPPP relationship in EBSD scans of figure 1(c-h)

Specimen	Volume fraction of ferrite	Total number of ferrite grains	Volume fraction of ferrite with type I LR deformation	Number of ferrite grains with type I LR deformation	Volume fraction of ferrite with type I LR deformation and CPPP relationship
IC750	0.67	124	0.16	21	0.14
IC775	0.44	79	0.03	4	0.01
IC800	0.07	42	-	-	-

block size and hence the minimum average PAGS as evident from Fig. 3(c). Small prior austenite grains generate the greatest elastic stresses upon transformation [28,29,31,32], hence forcing the surrounding microstructure to undergo plastic deformation to relax those stresses.

Limited freedom to choose variants for self-accommodation due to small PAGS forces the austenite to transform into martensite variants having CPPP relation with adjacent ferrite grains. This achieves relatively easy slip transmission while relaxing high transformation stresses resulting in type I LR deformation. An important implication of this is that ferrite grain orientation can affect the variant selection during the transformation of an adjacent small PAG [32,38].

The existence of the CPPP relation indicates an orientation relationship (OR) between intercritical ferrite and the austenite present before the transformation. As the intercritical temperature increases, the propensity of nucleating austenite to have K-S OR with multiple ferrite neighbors decreases [39]. Since boundaries without K-S OR grow faster [40,41], higher intercritical temperatures eventually result in microstructure with few austenite grains having K-S OR with ferrite neighbors. Therefore, a ferrite grain in DP steel has a higher probability of having K-S OR with multi-

ple prior austenite grains and hence CPPP relation with multiple martensite blocks if lower intercritical temperatures are used.

Ferrite-martensite interface boundary length can also determine the frequency of type I LR deformation. However, the interface boundary length decrease from 3195 μm in IC750 to 2970 μm in IC775 is very minimal and hence does not explain the drastic decrease in the frequency of type I LR deformation observed in IC775.

The fraction of ferrite grains with type II SR deformation is higher in IC750 than in IC775, but absent in IC800. This trend is opposite to the increasing martensite volume fraction in these specimens. Since type II SR deformation is observed in almost all ferrite grains where type I LR deformation is absent, it can be better explained by an overall average characteristic of the microstructure, rather than a local characteristic such as the fulfillment of CPPP relation.

Since the volumetric expansion of martensitic transformation increases with the increasing carbon content of martensite [42], it probably causes increased deformation in surrounding ferrite resulting in type II SR deformation. It seems that below a certain threshold carbon content, transformation strain is so low that the deformed ferrite layer is indistinguishable. Moreover, IC800 probably has a higher number of martensitic variants formed from a single prior austenite grain, as it has the largest prior austenite grain size. A higher number of variants can cancel the shear part of austenite-to-martensite transformation strain more effectively and significantly reduce the magnitude of deformation in ferrite [14,15]. Hence no type II SR deformation is observed in IC800.

In summary, there are two types of deformation observed in ferrite grains: a type I LR deformation that spans the complete ferrite grain, and a type II SR deformation in the form of a deformed ferrite layer at the ferrite/martensite boundary.

The fraction of ferrite grains with type I LR deformation was highest in specimen IC750 which has the smallest martensite block sizes, and hence smallest PAGS. When PAGS is small, austenite may transform into martensitic variants having a (110) CPPP relationship with neighboring ferrite. This enables effective relaxation of transformation stresses by relatively easy deformation of ferrite and results in type I LR deformation. It was observed that most ferrite grains with type I LR deformation also possess a (110) CPPP relationship with several surrounding martensite blocks.

At the locations where type I LR deformation and the CPPP relation are not observed, type II SR deformation is present. The carbon content in martensite should be sufficiently high so that the ferrite deformation caused by dilatation and shear of martensite is large enough to be measured by experiments. Moreover, a higher number of variants in specimens with large PAGS cancels the shear part of the transformation strain more effectively. Therefore type II SR deformation is observed only in IC750 and IC775 and is absent in IC800.

Declaration of Competing Interest

The authors declare that they have no known competing financial interests or personal relationships that could have appeared to influence the work reported in this paper.

Acknowledgments

This research was carried out under project number T17019j in the framework of the Research Program of the Materials innovation institute (M2i) (www.m2i.nl) supported by the Dutch government. We would like to thank Monika Krugla of Tata Steel for help and discussions regarding EBSD measurements.

References

[1] G. Krauss, Steels: Processing, Structure, and Performance, Second Edi, ASM International, Materials Park, Ohio, 2015.
[2] A. Nakagawa, G. Thomas, Metall. Trans. A 16A (1985) 831–840.
[3] R.G. Davies, Metall. Trans. A 10 (1979) 1549–1555.
[4] T. Sakaki, K. Sugimoto, Acta Metall 31 (1983) 1737–1746.
[5] D.L. Bourell, A. Rizk, Acta Metall 31 (1983) 609–617.
[6] D.A. Korzekwa, D.K. Matlock, G. Krauss, Metall. Trans. A 15 (1984) 1221–1228.
[7] U. Liedl, S. Traint, E.A. Werner, Comput. Mater. Sci. 25 (2002) 122–128.
[8] H. Mirzadeh, M. Alibeyki, M. Najafi, Metall. Mater. Trans. A Phys. Metall. Mater. Sci. 48 (2017) 4565–4573.
[9] M. Nouroozi, H. Mirzadeh, M. Zamani, Mater. Sci. Eng. A 736 (2018) 22–26.
[10] A. Karimi, S. Kheirandish, M. Mahmoudiniya, Kov. Mater. 55 (2017) 175–182.
[11] B.G. Prusty, A. Banerjee, Materials (Basel) 13 (2020) 556.
[12] Z. Xiong, A.G. Kostryzhev, Y. Zhao, E.V. Pereloma, Metals (Basel) 9 (2019) 1–14.
[13] M. Calcagnotto, D. Ponge, E. Demir, D. Raabe, Mater. Sci. Eng. A 527 (2010) 2738–2746.
[14] A. Ramazani, K. Mukherjee, U. Prahl, W. Bleck, Metall. Mater. Trans. A Phys. Metall. Mater. Sci. 43 (2012) 3850–3869.
[15] A. Ramazani, K. Mukherjee, A. Schwedt, P. Goravanchi, U. Prahl, W. Bleck, Int. J. Plast. 43 (2013) 128–152.
[16] A. Ramazani, K. Mukherjee, H. Quade, U. Prahl, W. Bleck, Mater. Sci. Eng. A 560 (2013) 129–139.
[17] J. Kadkhodapour, S. Schmauder, D. Raabe, S. Ziaei-Rad, U. Weber, M. Calcagnotto, Acta Mater 59 (2011) 4387–4394.
[18] T. Matsuno, R. Ando, N. Yamashita, H. Yokota, K. Goto, I. Watanabe, Int. J. Mech. Sci. 180 (2020).
[19] J. Moerman, P.R. Triguero, C. Tasan, P. van Liempt, Mater. Sci. Forum 702–703 (2011) 485–488.
[20] L. Ryde, Mater. Sci. Technol. 22 (2006) 1297–1306.
[21] D. Jorge-Badiola, A. Iza-Mendia, I. Gutiérrez, J. Microsc. 228 (2007) 373–383.
[22] M. Kamaya, A.J. Wilkinson, J.M. Titchmarsh, Acta Mater 54 (2006) 539–548.
[23] M. Kamaya, Mater. Charact. 66 (2012) 56–67.
[24] M. Kamaya, A.J. Wilkinson, J.M. Titchmarsh, 235 (2005) 713–725.
[25] S. Cheong, H. Weiland, Mater. Sci. Forum 558–559 (2007) 153–158.
[26] X.L. Wang, X.P. Ma, Z.Q. Wang, S. V Subramanian, Z.J. Xie, C.J. Shang, X.C. Li, 149 (2019) 26–33.
[27] S. Morito, H. Yoshida, T. Maki, X. Huang, Mater. Sci. Eng. A 438–440 (2006) 237–240.
[28] S. Morito, H. Saito, T. Ogawa, T. Furuhara, T. Maki, Acta Mater 63 (2018) 202–214.
[29] C. Celada-Casero, J. Sietsma, M.J. Santofimia, Mater. Des. 167 (2019).
[30] J. Hidalgo, M.J. Santofimia, Metall. Mater. Trans. A Phys. Metall. Mater. Sci. 47 (2016) 5288–5301.
[31] S. Takaki, K. Fukunaga, J. Syarif, T. Tsuchiyama, Mater. Trans. (2004) 45.
[32] S. Sakai, S. Morito, T. Ohba, H. Yoshida, S. Takagi, J. Alloys Compd. 577 (2013) S597–S600.
[33] J.P. Hirth, Metall. Trans. 3 (1972) 3047–3067.
[34] E.O. Hall, Proc. Phys. Soc. B 64 (1951) 747.
[35] E. Werner, W. Prantl, Acta Metall. Mater. 38 (1990) 533–537.
[36] I.J. Beyerlein, N.A. Mara, J. Wang, J.S. Carpenter, S.J. Zheng, W.Z. Han, R.F. Zhang, K. Kang, T. Nizolek, T.M. Pollock, JOM 64 (2012) 1192–1207.
[37] L. Patriarca, W. Abuzaid, H. Sehitoglu, H.J. Maier, Mater. Sci. Eng. A 588 (2013) 308–317.
[38] H. Yoshida, S. Takagi, S. Sakai, S. Morito, T. Ohba, ISIJ Int 55 (2013) 2198–2205.
[39] H. Sharma, J. Sietsma, S.E. Offerman, Sci. Rep. 6 (2016) 1–20.
[40] K. Chattopadhyay, Mater. Sci. Forum 3 (1985) 231–246.
[41] H. Dong, Y. Zhang, G. Miyamoto, H. Chen, Z. Yang, T. Furuhara, Scr. Mater. 188 (2020) 59–63.
[42] J.M. Moyer, G.S. Ansell, Metall. Trans. A 6 (1975) 1785–1791.